Available online at www.sciencedirect.com
ScienceDirect
Journal of Computational Physics 227 (2007) 1075–1093
JOURNAL OF COMPUTATIONAL PHYSICS
www.elsevier.com/locate/jcp

# A kinetic Monte Carlo method on super-lattices for the study of the defect formation in the growth of close packed structures

Massimo Camarda *, Antonino La Magna, Francesco La Via

*Consiglio Nazionale delle Ricerche, Istituto di Microelettronica e Microsistemi, CNR-IMM, Stradale Primosole 50, I-95121 Catania, Italy*

Received 2 April 2007; received in revised form 31 July 2007; accepted 21 August 2007
Available online 20 September 2007

**Abstract**

A modified Kinetic Lattice Monte Carlo model has been developed to predict growth rate regimes and defect formation in the case of the homo-epitaxial growth of close packed crystalline structures. The model is an improvement over standard Monte Carlo algorithms, which usually retain fixed atom positions and bond partners indicative of perfect crystal lattices. Indeed, we extend the concepts of Monte Carlo growth simulations on super-lattices containing additional sites (defect sites) with respect to those of the reference material. This extension implies a reconsideration of the energetic mapping, which is extensively presented, and allows to describe a complex phenomenology that is out of accessibility of standard stochastic approaches. Results obtained using the Kawasaki and the Bond-Counting rules for the transition probability of the Monte Carlo event are discussed in details. These results demonstrate how the defect types (local or extended), the formation mechanisms and the defect generation regimes can be characterized using our approach.


*PACS:* 61.72.Bb; 68.35.Ct; 81.10.Aj; 81.15.Aa

*Keywords:* Kinetic Lattice Monte Carlo; Island nucleation; Defective epitaxial growth

## 1. Introduction

The problematic of the epitaxial crystal growth of materials having close packed crystalline structures is tightly connected to the polytypism (a special case of one-dimensional polymorphism) [1] that such materials usually show. Indeed, close packed crystals can have a high degree of stable crystal configurations with the same chemical composition, a similar content in terms of bulk free energy but a different one-dimensional stacking and different physical and electrical properties. This effect is related to the two possible equivalent sites for the atom sticking on the crystal surface during the deposition process.

* Corresponding author. Tel.: +39 0955968238.
*E-mail address:* camarda.massimo@gmail.com (M. Camarda).

0021-9991/$ - see front matter 
doi:10.1016/j.jcp.2007.08.036

In order to reduce polytype mixing, surface steps can be formed by off-axis cuts of the substrate, thus forcing the epitaxial grown layer to inherit the polytype of the substrate. This technique is known as "step controlled homoepitaxy" [2,3]. This homo-epitaxial step-flow growth contrasts the nucleation and growth of islands of complementary symmetry with respect to that of the substrate which would, eventually, lead to the formation of polycrystalline structures. Island nucleation increases at higher deposition rates; therefore, imposing a low growth rate in the experimental setting is the usual empirical prescription to avoid the polycrystalline growth regime. Indeed, when the time interval between two successive deposition events in the same terrace area is much larger than the average time which the adatom spends in the terrace before encountering the step (diffusion limited regime), an optimal homo-epitaxial growth should occur. Several deposition parameters can influence the quality of the grown crystal (i.e. temperature, off-angle cut, precursor flows, etc.); as a consequence, a deeper understanding of the possible defect formation mechanisms can help to increase the growth rate limit allowing for cheaper epitaxial processes.

In the past the problem of island nucleation and evolution in the homo-epitaxial step-flow growth was studied applying analytical models based on the theory of Burton et al. [4] for the dynamics of the step together with the Avrami nucleation theory [5] or using on-lattice numerical methods (Kinetic Lattice Monte Carlo (KLMC) [6]). Each method has its own advantages and limits. The BCF theory is a continuous theory which correctly accesses the time and length scale of the process (microns and seconds) but it misses the atomic scale description, whereas the limit of standard on-lattice methods is that the kinetic particles (adatoms, terrace atoms and atoms in the bulk) reside in the characteristic lattice sites of the material in study, so that they fail on describing the generation and evolution of defects. On the other hand, off-lattice methods (ab initio [7], molecular dynamics [8] and Monte Carlo [9]), can be successfully used for the study of defects but are unable to reach the time scale of the epitaxial process (seconds). More generally, using standard kinetic schemes, only particular topics of the growth kinetics can be theoretically investigated, since they fail in describing the correlation between the concurrent aspects characterizing the micro-structural evolution of the system (island nucleation, correlation between the evolution of islands with different symmetry, correlation between the island and step evolution, interaction between bulk and surface structures) on the correct time scale of the process.

The goal of this work is to develop an innovative method for the investigation of the growth process kinetics in the case of close packed structures which allow, in principle, to access to the full complexity of the phenomenology in study. The method extends the concepts of the Kinetic Lattice Monte Carlo growth simulation on super-lattices containing additional sites with respect to those of the reference lattice of the material in study [10]. This extension allows to describe the generation and evolution of defects at the atomic level but, also, to overcome the time scale limits typical of the off-lattice methods.

The paper is structured as follows. In Section 2, we introduce the refined lattice used, specifying bonds and neighbors. Section 3 specifies the probability rules used for the adatoms evolution. In Section 4, we discuss the different possible boundary conditions, defining the *Helicoidal Boundary Conditions*. The deposition algorithm, used in the epitaxial process, is specified in Section 5. In Sections 6 and 7, we present the results for the two-dimensional (2D) and three-dimensional (3D) cases, respectively. In Section 8 we, finally, discuss the main results obtained.

## 2. Numerical methodology

In the *KLMC* method the lattice is represented by a structured mesh which fixes the allowed atom positions and bond partners. In order to achieve the possibility of representing and considering in the evolution algorithm the dynamics of the defective structures we use, as substrate of our *KLMC* model, a refined effective lattice including the real lattice sites of the close packed structure as a sub-lattice. In particular, we use a hexagonal lattice with reduced inter-site distance with respect to the one of the regular lattice. In this refined lattice, second-neighbors are generally associated to the regular relative positions of the close packed structure in study, whereas first-neighbors are associated to defective configurations. Considering a given (0001) layer, this choice allows us to consider all the three possible different adatoms occupation sites (generally called A, B and C) as sites of the hexagonal structure (see Fig. 1), while a single kind of site (A or B or C) is occupied in the regular lattice. The use of a refined lattice implies that:

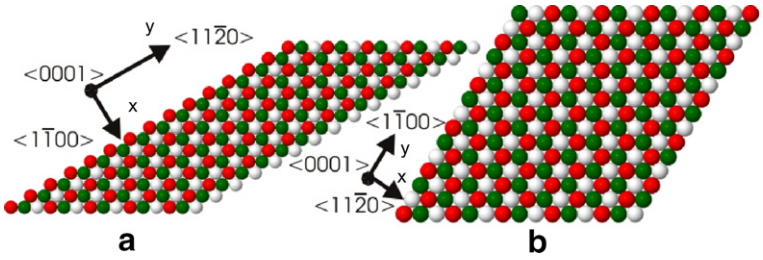


Fig. 1. View of a (0001) layer of our refined lattice for $\langle 1\bar{1}00\rangle$ (a) and $\langle 11\bar{2}0\rangle$ (b) off-angle cut directions. Each site (either A, B and C) is differently colored. The particle on the $y$ direction has the same configuration/symmetry of the ideal step. It can be seen that in (a) the particles in the border have four bonds with the next-neighbors of the same type, while in the case (b) only three bonds are present. This last case represents a less stable configuration for the step.

(1) in general, only 2/3 of the memory allocated for the lattice is made up of empty sites (if defects are absent);
(2) all the different poly-types (both cubic and hexagonal, mono and poly crystalline structures) can be described in terms of the same basic lattice, changing only the rules for the site filling;
(3) the hexagon formed by next-neighbors (i.e. the hexagon of the regular lattice) is rotated 30° with respect to the closer one made up of first-neighbors.

In relation to the last point we note here that, in the simulation of the step-flow growth, the symmetry of the lattice should respect the symmetry of the step; otherwise the boundary conditions (either normal or helicoidal ones) cannot be correctly applied (see also Section 4). Therefore, if we choose to make "on angle" cuts for the step directions, we have only two non-equivalent directions in a hexagonal lattice (Fig. 1):

- one is the direction connecting either two first-neighbors, which corresponds to the $\langle 1\bar{1}00\rangle$ off-angle cut (Fig. 1a). With this choice we have the following primitive vectors $\widehat{X}, \widehat{Y}, \widehat{Z}$:

$$\begin{aligned} \widehat{X} &= \left(A_1 + \frac{3}{2}A_2\right)\hat{x} \\ \widehat{Y} &= \frac{\sqrt{3}}{2}A_2\hat{y} \\ \widehat{Z} &= A_3\hat{z} \end{aligned} \tag{1}$$

Here $A_1$, $A_2$ and $A_3$ are integer numbers in the range $[1, \mathrm{Len}_x]$ $[1, \mathrm{Len}_y]$ $[1, \mathrm{Len}_z]$, respectively, defining the extension of the computational box, and $\hat{x}, \hat{y}, \hat{z}$ are the standard Cartesian versors. The inter-site distance $a$ in the refined lattice is set equal to the unity. These vectors generate a simple hexagonal Bravais lattice where each site type can be identified using the following conditions:

$$\begin{aligned} &\mathrm{MOD}(A_1 + 0, 3) = 0 \Rightarrow \mathrm{TypeA} \quad \text{(colored white)} \\ &\mathrm{MOD}(A_1 + 1, 3) = 0 \Rightarrow \mathrm{TypeB} \quad \text{(colored green)} \\ &\mathrm{MOD}(A_1 + 2, 3) = 0 \Rightarrow \mathrm{TypeC} \quad \text{(colored red)} \end{aligned} \tag{2}$$

- the other is the direction connecting two next-neighbors, this corresponds to the $\langle 11\bar{2}0\rangle$ cut, which is rotated of 30° with respect to the first one (Fig. 1b). With this choice, we then have the following primitive vectors:

$$\begin{aligned} \widehat{X} &= \left(A_1 + \frac{1}{2}A_2\right)\hat{x} \\ \widehat{Y} &= \frac{\sqrt{3}}{2}A_2\hat{y} \\ \widehat{Z} &= A_3\hat{z} \end{aligned} \tag{3}$$

and the following conditions:

$$\begin{aligned} &\mathrm{MOD}(A_1 + A_2 + 0, 3) = 0 \Rightarrow \mathrm{TypeA} \quad \text{(colored white)} \\ &\mathrm{MOD}(A_1 + A_2 + 1, 3) = 0 \Rightarrow \mathrm{TypeB} \quad \text{(colored green)} \\ &\mathrm{MOD}(A_1 + A_2 + 2, 3) = 0 \Rightarrow \mathrm{TypeC} \quad \text{(colored red)} \end{aligned} \tag{4}$$

In Section 7, we will show the effects of the step direction on the step dynamics and stability. Here, we can anticipate that the $\langle 1\bar{1}00\rangle$ choice for the step direction is the most stable one, since the regular coordination number for the adatoms bounded to the step is four, while the coordination of the step adatom is three in the $\langle 11\bar{2}0\rangle$ case (Fig. 1).

In both representations we consider up to 26 possible neighbors, but the triples of integers identifying these neighbors are not the same. Therefore, we keep them in separated lists (see Fig. 2):

Second-neighbors in the same plane k (Fig.2a):

| $\langle 11\bar{2}0\rangle$-STEP | $\langle 1\bar{1}00\rangle$-STEP |
|---|---|
| (i+1,j+1,k+0) (i-1,j+2,k+0) (i-2,j+1,k+0) | (i+0,j+1,k+0) (i-3,j+2,k+0) (i-3,j+1,k+0) |
| (i-1,j-1,k+0) (i+1,j-2,k+0) (i+2,j-1,k+0) | (i+0,j-1,k+0) (i+3,j-2,k+0) (i+3,j-1,k+0) |

First-neighbors in the same plane k (Fig.2b):

| $\langle 11\bar{2}0\rangle$-STEP | $\langle 1\bar{1}00\rangle$-STEP |
|---|---|
| (i+1,j+0,k+0) (i-0,j+1,k+0) (i-1,j+1,k+0) | (i+1,j+0,k+0) (i-1,j+1,k+0) (i-2,j+1,k+0) |
| (i-1,j-0,k+0) (i+0,j-1,k+0) (i+1,j-1,k+0) | (i-1,j+0,k+0) (i+1,j-1,k+0) (i+2,j-1,k+0) |

and, finally, the first-neighbors in the lower (k-1) and upper (k+1) plane respectively (Fig.2c and Fig.2d):

| $\langle 11\bar{2}0\rangle$-STEP | $\langle 1\bar{1}00\rangle$-STEP |
|---|---|
| (i+1,j+0,k-1) (i-0,j+1,k-1) (i-1,j+1,k-1) | (i+1,j+0,k-1) (i-1,j+1,k-1) (i-2,j+1,k-1) |
| (i-1,j-0,k-1) (i+0,j-1,k-1) (i+1,j-1,k-1) | (i-1,j-0,k-1) (i+1,j-1,k-1) (i+2,j-1,k-1) |
| (i+0,j-0,k-1) | (i+0,j-0,k-1) |
| (i+1,j+0,k+1) (i-0,j+1,k+1) (i-1,j+1,k+1) | (i+1,j+0,k+1) (i-1,j+1,k+1) (i-2,j+1,k+1) |
| (i-1,j-0,k+1) (i+0,j-1,k+1) (i+1,j-1,k+1) | (i-1,j-0,k+1) (i+1,j-1,k+1) (i+2,j-1,k+1) |
| (i+0,j-0,k+1) | (i+0,j-0,k+1) |

Considering all these possible neighbors we have the 26 possible bonds for the adatom (Fig. 3).

## 3. Evolution algorithm

The evolution in the *KLMC* approach can be described as a stochastic sequence of elementary atomic displacement events for the Monte Carlo particles. Therefore, a particle residing at site $i$ can potentially move to a site $j$ and this displacement is governed by a given probability rule $P_{ij}$, which is related to the relative stability of the two configurations. Setting $P_{ij}$ for a given material is not an easy task since, even restricting the effective interactions to close-neighbors, a large number of $P_{ij}$ values should be considered ($2^{Np}$ possibilities in our case if symmetries are not considered, being $Np$ the sum of the number of neighbors of the $i$ site plus the number of neighbors of the $j$ site which are not neighbors of the $i$ site) and the use of lookup tables would be mandatory [11]. Although the method presented here, applied to a particular material, can be easily generalized to the use of lookup tables, this is far away from the purpose of the present manuscript.

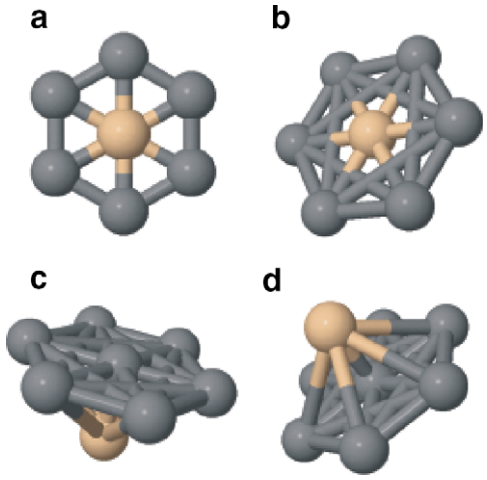


Fig. 2. Neighbors on the different planes.

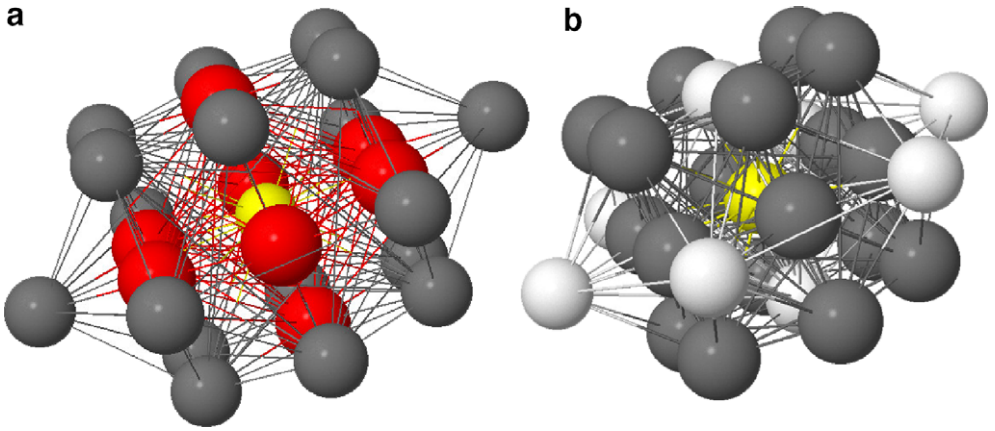


Fig. 3. (a) Neighbors of the central site (yellow sphere) contributing to its energetics in our KLMC method. Red spheres indicate first-neighbors while gray spheres indicate next-neighbors. (b) Possible diffusion directions (gray spheres) for a Monte Carlo particle sitting at the central site (yellow sphere).

We, instead, use a simplified probability rule based on the contribution of two kinds of bonds forming between first-neighbors or next-neighbors respectively. As we have already stated, in our model up to 26 neighbors can in principle contribute to the adatom stability (Fig. 3a). Each red atom (up to 8) contributes to a "defective" bond and the related bonding energy $E_{\text{defect}}$ (the energy which must be given to the system in order to break the bond) can eventually be negative, whereas the gray atoms (up to 18) contribute to a "regular" bond and the related bonding energy $E_{\text{regular}} = E_{\text{B}}$ is always positive. The ratio $R_{\text{s}} = E_{\text{regular}}/E_{\text{defect}}$ is an important parameter of the simulation which is directly related to the surface energy of the defects and, as we will see, can limit the allowed elementary displacements. Again, this phenomenological parameter should be estimated with the aid of experimental data or through molecular dynamics. Without loosing generality, in the results presented in this work we fix the value to $R_{\text{s}} = -2.2$. We have also performed simulations (not shown) with different $R_{\text{s}}$ values and we realize that the qualitative behavior of the system kinetics does not change substantially when $R_{\text{s}}$ is negative. A relevant change in the simulation results is observed for a positive value of $R_{\text{s}}$ related to the high density of defects in interstitial positions. However, the physical relevance of the simulation results with $R_{\text{s}} > 0$ (which favors the creation of highly compact structures) should be carefully evaluated, eventually considering particular applications.

Assuming that the bond strength does not depend on the bond network in a given configuration, we can have two possible choices of $P_{ij}$ which in turn satisfy the detailed balance rule:

$$P_{ij} = \nu_{\mathrm{Kaw}} \exp\left\{\beta E_{\mathrm{B}}\left[\left(n_i^{\mathrm{a}} - n_j^{\mathrm{a}}\right) + R_{\mathrm{s}}\left(n_i^{\mathrm{r}} - n_j^{\mathrm{r}}\right)\right]\right\} \quad \texttt{Kawasaki Rule (KawR)} \tag{5}$$

$$P_{ij} = \nu_{\mathrm{Bc}} \exp\left\{\beta E_{\mathrm{B}}\left(n_i^{\mathrm{a}} + R_{\mathrm{s}} n_i^{\mathrm{r}}\right)\right\} \quad \texttt{Bond-counting Rule (BcR)} \tag{6}$$

where $(n_i^{\mathrm{a}}, n_i^{\mathrm{r}})$ and $(n_j^{\mathrm{a}}, n_j^{\mathrm{r}})$ are the number of regular and defective bonds for the initial and final sites. In this work we have used these two rules which seem to differ mainly for the effective kinetics which are faster for the Kawasaki rule.

Several considerations have to be taken into account when applying these rules to the refined lattice. The *BcR* starts from the statement that the energy barrier for a given displacement is independent of the final configuration, depending only on the energy difference between the initial bounded site and the free particle's energy; this rule, in turn, is based on the assumption (which is indeed true for meshes coinciding with the regular lattice) that the energy for the final bounded configuration is always lower than the free particle's one. This assumption is not always true in our case (e.g. $E(n^{\mathrm{a}} = 0, n^{\mathrm{r}} = 0) = E_{\text{free particle}} < E(n^{\mathrm{a}} = 0, n^{\mathrm{r}} = 1)$ when $R_{\mathrm{s}} < 0$). Therefore, in order to correctly implement the *BcR*, we then have either to exclude these unstable sites from the list of possible movements or renormalize the energy barrier with respect to the most unstable site configuration. However, the last choice would assign an unphysical negative energy to the free particle. On the base of this discussion, we can define a stable destination site as a site where $E(n^{\mathrm{a}}, n^{\mathrm{r}}) < E_{\text{free particle}}$ is verified. Since $\mathrm{E}(n^{\mathrm{a}}, n^{\mathrm{r}})$ depends on the $R_{\mathrm{s}}$ value, the possible allowed destination sites will depend on this parameter too. More specifically, the allowed sites in the *BcR* are those where $n^{\mathrm{a}}$ and $n^{\mathrm{r}}$ satisfy the following equation:

$$n^{\mathrm{a}} + R_{\mathrm{s}} n^{\mathrm{r}} > 0. \tag{7}$$

Having defined a rule to calculate the relative energetics between two configurations, we have to determine the list of the possible allowed transitions for a given particle $i$. In general, when considering stochastic sequences of elementary lattice displacements in *KLMC*, it is more efficient and accurate to consider only one set of displacements (the smallest possible ones) whose probability is directly connected to the diffusion coefficients of the adatom. Moreover, these elementary displacements should allow the particles to effectively span the whole system. We separate our discussion for displacements along the $x$–$y$ plane and along the $z$ direction. Since we know that, on a flat layer along the $x$–$y$ plane, complementary sites are energetically equivalent, we allow the particle to move only between these first-neighbors. This choice lets the system explore different globally stable morphologies, i.e. create islands and defects, and allows us to study their interaction with the steps. On the other hand, the shortest possible diffusion along the $z$ direction is $x \to x$, $y \to y$, $z \to z \pm 1$, but this choice creates an effective barrier for vertical diffusion, which inhibits three-dimensional island melting. Thus movements $i \to j$ to complementary sites (e.g. if $\mathrm{Type}(i) = \mathrm{A}$ the allowed site will be $\mathrm{Type}(j) = \mathrm{B}$ or C) are the most natural and physical choices for all directions. On the basis of these considerations we restrict the final site $j$ to be one of the 18 of 26 neighbors, belonging to the complementary type with respect to the site $i$. The list of the allowed sites includes the six next-neighbors in the same plane of the site $i$ and the corresponding sites in the upper and lower plane (see Fig. 3b). We have used the Continuous Time algorithm [12] for the selection of the event sequence and the time interval between two subsequent events. The random number generator used is the "Mersenne Twister" [13].

## 4. Boundary conditions

In order to reduce finite size effects we must use boundary conditions along the growth plane, i.e. along the step direction ($y$) and perpendicularly to it ($x$). The most commonly used boundary conditions are the "Periodic Boundary Conditions" (*PBCs*). However this choice has strong limitations on this particular system. In fact, in order to correctly apply the *PBCs* along the $x$ direction we should make the system symmetric around its middle point ($\mathrm{Len}_x/2$). This can be done representing an even number of left and right steps, thus making the substrate look like a "hill" (Fig. 4a) [6]. Using these conditions along $x$ and $y$ (of course not along $z$) we have

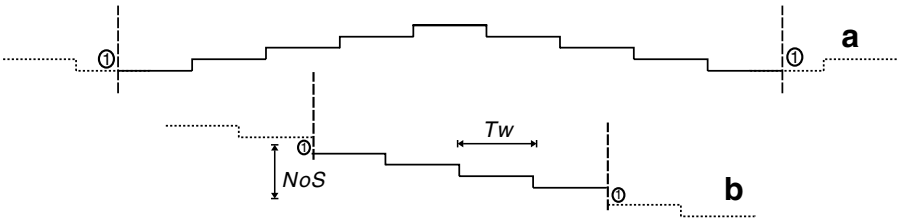


Fig. 4. The two possible initial substrates, based on the boundary conditions used: (a) standard periodic boundary conditions and (b) helicoidal boundary conditions.

$$\begin{aligned} x &= \mathrm{MOD}(Len_x + x, Len_x) \\ y &= \mathrm{MOD}(Len_y + y, Len_y) \\ z &= z \end{aligned} \tag{8}$$

As a consequence *PBCs* have two important disadvantages:

- the growth is limited to the number of layers of the initial substrate. Indeed, the growth on top of the hill cannot be considered part of the growth process being "step-free". This means that in order to grow, for example, 100 layers of the $4H$ polytype we would need a lattice with extension $L_x = 100 \times 4 \times$ Terrace Width, where Terrace Width is the distance between the steps. This extension should be compared to $L_x = 4 \times$ Terrace Width for the case with helicoidal boundaries (discussed later).
- during the simulation the terrace width will "naturally" decrease. In fact, as soon as the lower layer is completed, its terrace width reduces to zero, then the next lower terrace width will reduce to zero and so on. This is not what happens during the step-flow growth [2]. This disadvantage is even more relevant being the terrace width an important parameter which strongly influences the final morphology of the crystal growth. In other words using these boundary conditions the effective terrace width is lower than the one of the substrate.

Given these two important limitations we have decided to use what we called "Helicoidal Boundary Conditions (*HBC*)" along $x$, together with standard periodic ones along $y$. With these boundary conditions we have the following relations:

$$\begin{aligned} x &= \mathrm{MOD}(Len_x + x, Len_x) \\ y &= \mathrm{MOD}(Len_y + y, Len_y) \\ z &= \begin{cases} z & \text{if } 0 < x < Len_x - 1 \\ z + \text{Number of Steps } (NoS) & \text{if } x \geqslant Len_x \\ z - \text{Number of Steps } (NoS) & \text{if } x < 0 \end{cases} \end{aligned} \tag{9}$$

where *Number of Step* is the total number of the steps on the initial substrate. This choice assumes the equivalence between the lowermost and uppermost terrace (see Fig. 4b) as it should occurs in an ideal step-flow growth and it is not affected by the *PBCs* problems when applied to the step-flow growth conditions. This fact allows us to growth any number of layers irrespective of the number of layers of the initial substrate, which can be kept to the minimum necessary (Fig. 4b).

## 5. Deposition algorithm

The deposition algorithm defines the way particles are incorporated into the system and it strongly influences the final morphology of the grown crystal. Before describing the different deposition algorithms we need to define the *Surface Sites* (*SS*).

- A site ($A_1$, $A_2$, $A_3$) is a *SS* if it is empty and has at least one dangling bond which an atom can connect to. This atom will stabilize the configuration by lowering its energy, thus becoming an adatom (this means that, when $R_s$ is negative, the *SS* types will be complementary to the type of the underlying layer).

Given this definition we can implement two different algorithms:

(1) use of an array to keep track of all the *SSs* present into the lattice so that, every time the deposition event is called, a *SS* site can be randomly extracted and occupied. This choice can be used in case of hot and rarefied gases (plasmas), and it gives equal impingement probability to "hills" and "valleys" thus promoting flat surfaces in grown crystal.
(2) for each deposition event a site is randomly chosen from the top layer ($Len_z$), then the particle diffuses downward to the surface of the crystal by means of a sequence of random jumps, the direction of these jumps is chosen among the allowed ones using an appropriate probability distribution. This algorithm could reproduce the collisions among free particles in the gas and the eventual presence of drift forces. Therefore, it can simulate gases at different temperatures and densities, and the conditions of the electrical field assisted deposition. Of course, in general, this choice will give different probabilities to "hills" and "valleys" thus promoting rougher crystal surfaces.

We have implemented both methods, but we focused our attention on the second one being more flexible and able to describe different deposition conditions. It must be noted that algorithm (1) is a special case of (2) where the downward drift force is set to infinity (i.e. the probability distribution is a delta function in the force direction) so that only downward vertical movements are considered during the diffusion of the free particle. Furthermore, the strict use of the algorithm (1) results in an unphysical non-zero probability for a fictitious deposition inside voids eventually present inside the bulk crystal. Given these two restrictions, we have decided to use only the second type of deposition algorithm. Moreover, in the results presented in this work we have set, without losing in generality, the random walk probability distribution in the gas, fixing to zero the probability for upward jumps and giving the same probability for downward jumps [6].

## 6. Results for the two-dimensional case

In order to better elucidate the model's capability to address the structural defects' problem in the growth of close packed materials, we start to study the evolution at constant temperature of two-dimensional systems. In Fig. 5, we show snapshots of the evolution of two systems, having equal size, governed by the two probability rules. We initialized the simulations starting with a layer on the (0 0 0 1) surface fully occupied with one site type (e.g. A type), then 10% of the second layer *SSs* (which are, by definition, the complementary sites of the first layer, i.e. B or C sites) are randomly filled. Afterwards (for the two cases in study) the system evolution

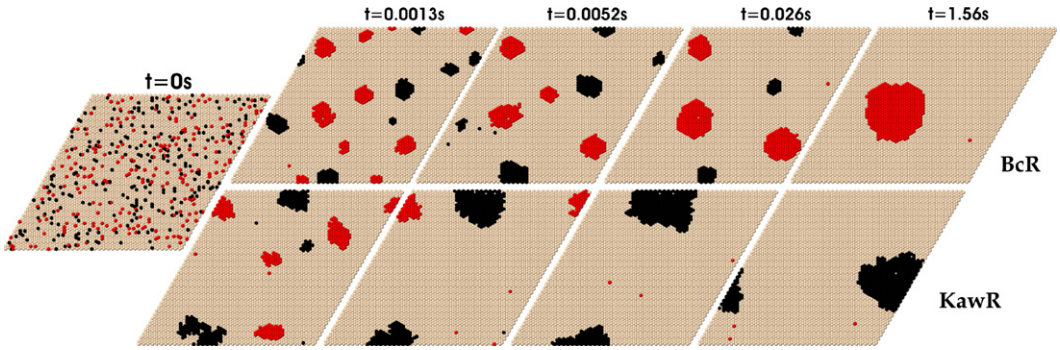


Fig. 5. 2D evolution for BcR and KawR methods. The islands in the BcR evolve along almost stable (hexagonal) configurations, whereas in the KawR one islands tend to evolve faster and maintain a rougher boundary. The physical parameters of both simulations are: $\beta E_b = 3.553$ and $R_s = 2.2$ $\nu_{Bc} = 10^{13}$ Hz. Red, black and light brown atoms are associated to the three possible site types A, B and C.

toward stable configurations has been monitored. In order to compare formally equivalent results obtained by the two methods we set, here and in the following, $\nu_{\mathrm{Kaw}} \equiv \nu_{\mathrm{Bc}}\exp(-3\beta E_{\mathrm{b}})$ and $\nu_{\mathrm{Bc}}$ equal to the nominal value $\theta_{\mathrm{D}} = 10^{13}$ Hz of the system Debye frequency. We note that this choice will give the same diffusion probability $P_{ij}$ for an adatom residing on a flat terrace.

As we can see in Fig. 5, due to the encounter events between the diffusing adatoms, the particles will tend to form small islands of the two complementary symmetries with respect to that of the underlying layer. After the nucleations, occurring at a very small time scale, larger aggregates form by means of two eventually concurrent mechanisms: (a) the Ostwald ripening and (b) the merging. Indeed the average island size grows, both, due to the exchange of diffusing monomers from small to large aggregates (a) and due to islands diffusion and merging (b). Therefore, the interaction between islands of the same or different symmetry can be indirect (i.e. mediated by the monomers released by the islands) and direct (after a merging event). We note that, while the Ostwald ripening mechanism acts equivalently for islands with same and different symmetry (since monomer can diffuse with the same probabilities through the sites complementary to that of the underlying layer), the merging events between islands with different symmetry follow different, slower, kinetics. We, finally, note that the merging mechanisms between two islands have strong similarities with the interaction events between steps and islands in the case of 3D growths discussed in the following section.

In Fig. 6, we show the total energy evolution of the adatom system for the two simulations shown in Fig. 5. Both the visual analysis and the equilibration trend of the total energy indicate that the system ruled by the KawR evolves faster toward the steady state. Indeed, the system reaches the configuration of single large island after $\sim$0.026 s in the case of the KawR while a similar configuration is reached after $\sim$1.2 s by the system ruled by the BcR. Moreover, the island morphology is clearly different since the tendency of aligning the island borders along the low energy $\langle 1\bar{1}00\rangle$ direction is more noticeable in the BcR case with respect to the KawR case; and, consequently, the borders are rougher for systems ruled by the KawR. Of course, the equilibration features and the island morphology are related. A rough interface indicates a globally lower stability for adatoms located at the island borders and, as a consequence, a boosting of the two growing mechanisms (a) and (b) due faster adatom detachments (a) and reconfiguration (b).

It is worthwhile to note that the usual considerations [14] regarding the difference between the two algorithms in computing the border adatoms diffusion loose their validity when using a refined lattice. In particular, if the KLMC lattice coincides with the standard lattice, the KawR sets the same diffusion probability for an adatom sitting at an island border and for a free adatom on a terrace [14]. Our method results in different border adatom kinetics. In fact, having extended the possible displacements to defective sites, the possible displacements of an atom bounded to an island border lead to the breaking of one or more stable bonds $E_{\mathrm{regular}}$ without any compensation. This makes the displacement probability of a border adatom for the KawR similar

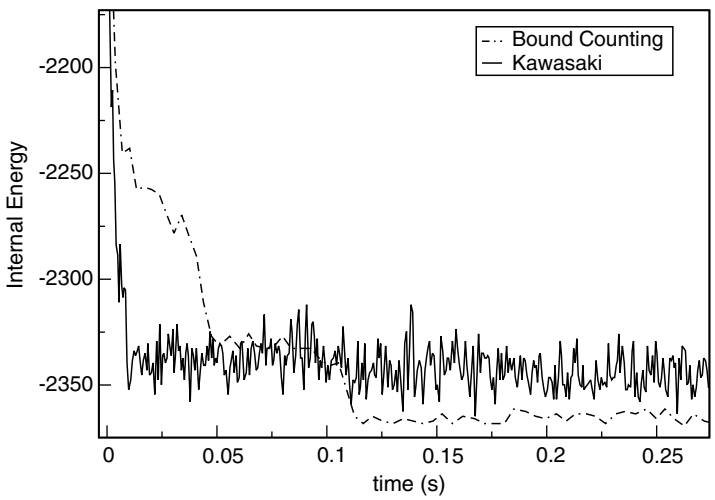


Fig. 6. Internal energy (in units of $\beta E_{\mathrm{b}}$) flow for the two methods at the same temperature and starting from a random configuration.

to that obtained in the case of the BcR (i.e. the diffusivity of a border adatom is significantly lower than the diffusivity of a terrace atom). As a consequence, the differences between the global kinetic of the step obtained with the two methods derive from many particle effects rather than from the different local diffusion rates of the single particles.

## 7. Results for the three-dimensional case

We can now turn our attention to the numerical study of the deposition process for the 3D case. In this case, the kinetics is influenced by many concurrent effects such as the deposition events, the lateral and vertical growth of the steps and the eventual interaction between the step and islands of complementary type.

We have studied several deposition conditions fixing the energetic ($\beta E_b = 3.553$ and $R_s = -2.2$) and varying: the geometry (off-angle cut value, direction and polytype of the initial substrate), the growth rates (in units of a nominal value $\theta_D = 10^{13}$ Hz of the Debye frequency of the system), the temperature and the evolution algorithm (using the KawR and the BcR). Finally, when not explicitly stated, we have fixed the off-angle cut along the $\langle 1\bar{1}00\rangle$ direction being the most stable and used one [15]. We begin by considering deposition conditions where polycrystalline growth occurs. In Fig. 7, we show both the initial substrate (a) and final grown film (b) for a low off-angle cut (Terrace Width (Tw) equal to 30 in units of the refined lattice first-neighbors distance) and an high deposition rate ($Gr = 1.73 \times 10^{-9}$ in units of the Debye frequency $\theta_D$ and of the inter-site distance $a$). Using these conditions we can observe island nucleation and, consequently, the interaction between islands and steps. It is worth noting that the interaction mechanism between the islands and the step is different from the one between two islands in the two-dimensional case, since in the 3D epitaxial growth the step has an effective drift velocity (lateral velocity) toward the island so that the principal interaction between the two structures is the merging rather than the Ostwald ripening mechanism.

In our simulations we have observed that, if the step reaches an island having the same symmetry, a fast reconfiguration of the island particles in the step structure occurs. This encounter event does not practically alter the effective evolution of the step. In turn, when the step reaches an island of complementary type two scenarios are possible: either the step imposes a modification on the island type to reproduce its stacking sequence or, if the island is too big and consequently too stable, it wraps around it. In the latter case the islands can potentially initiate the vertical growth of a local fault in the stacking sequence and, eventually, generate an extended polycrystalline structure. In relation to these scenarios it is important to note that, in either cases, the encounter strongly modifies the effective step kinetics causing a deformation of the step which, in turn, favors the creation of other defects in the surface.

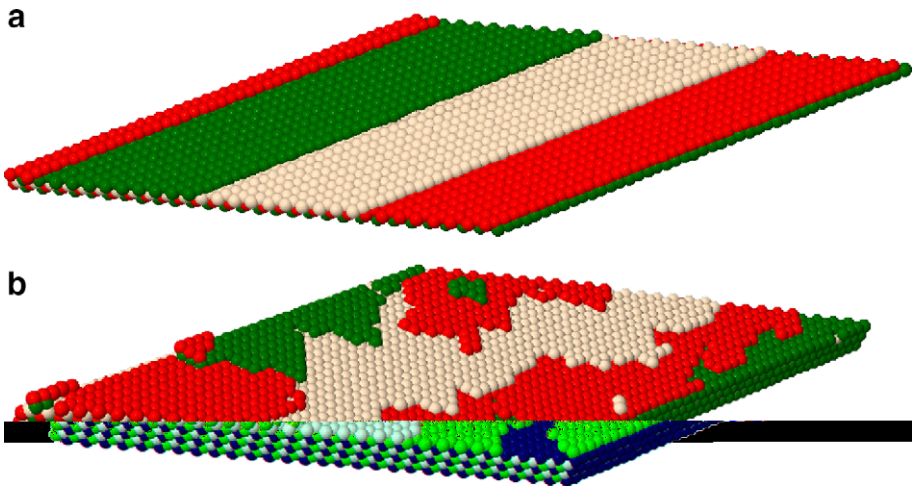


Fig. 7. Highlight of the surface morphology for 3D deposition simulation using the Bond Counting method and a fast deposition rate (see the text). The initial system has an impingement surface made up of $87 \times 45$ particles, distributed in three large terraces of 30 units wide, the polytype substrate is 3C.

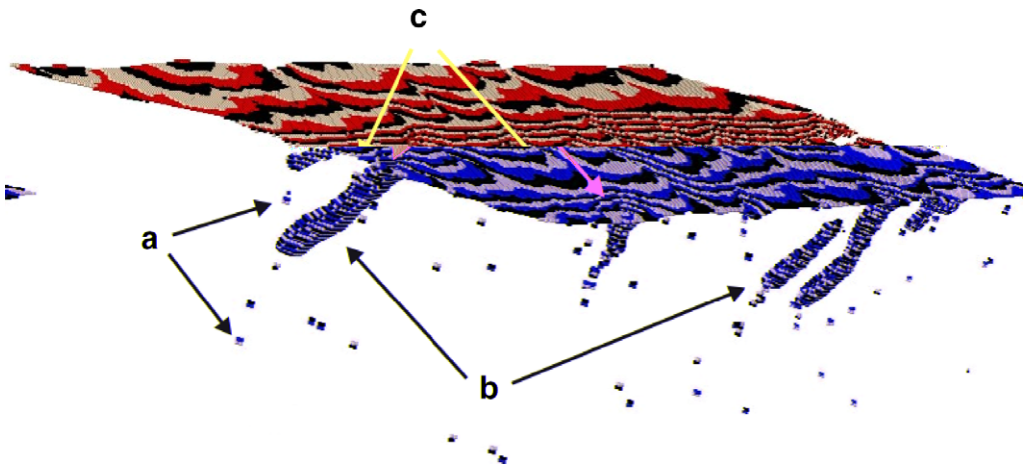


Fig. 8. Kinetic particles (i.e. both defects and adatoms) resulting from a polycrystalline growth of 150 layers, both local (A) and extended (B) defects are present. The influence of extended defects on the surface is shown (C). The system has a surface made up of $864 \times 864$ sites (refined lattice) distributed over 52 flat terraces, respectively, 18 units wide. The deposition rate was set equal to $Gr = 7 \times 10^{-10}$.

In Fig. 8, we show the kinetic particles (i.e. both defects and adatoms) resulting from a polycrystalline regime growth of 150 layers (we do not display bulk particles for graphical convenience). Free vacancies (a) and extended 3D defects resulting from the vertical growth of a microcrystalline structure with the wrong stacking sequence (b) are present. We note that the presence of extended defects in the crystal bulk strongly alters the surface morphology (c). *Vice versa*, the evolution of the surface morphology has a strong impact on the internal structure of the crystal, so that, surface morphology can be used as a signal of a change in the growth regime.

In addition to the formation of 3D extended defects two other main mechanisms can influence the surface morphology: the Local Step Bunching (*LSB*) and the Global Step Bunching (*GSB*). These mechanisms are connected to the kinetics of the steps and to the interaction among them through the diffusing adatoms. Local Step Bunching occurs when, due to thermal fluctuations and deposition randomness, the deformations of the steps become of the order of half the terrace width so that the steps will bunch locally with the adjacent ones. This deformation, which does not alter the average terrace width but only its variability, favors the creation of local defects associated with local unstable configurations. This process strongly depends on both the deposition rate and on the off-angle cuts (note that lower cuts mean larger terraces so that the steps have to deform significantly in order to intercept the neighbor ones).

*GSB*, on the other hand, is connected to global variations on the lateral velocity of subsequent steps which can derive both from intrinsic differences of the step structure or by interactions among the steps (i.e. repulsion or attraction [16,17]). Indeed, it has been shown [6,20–22] that only hexagonal polytypes manifest this mechanism for large terraces (i.e. when the interaction among the steps is virtually suppressed) whereas cubic ones do not show *GSB*. This is what happens in our simulations as it can be seen in Fig. 9, where we show the $\langle 0\,0\,0\,1 \rangle$ surface morphology of two grown crystals under the same deposition conditions changing only the initial substrate from cubic 3C polytype (a) to hexagonal 4*H* polytype (b). The *GSB* is an important limiting effect for the growth of high quality crystals since it effectively increases the average terrace width (see terraces on the left side of Fig. 10), thus increasing also the 2D nucleation probability and, as a consequence, the probability of polytype mixing. This can, in part, explain the higher probability of creating 3C monocrystals in comparison with 4H and 6H observed for the epitaxial growth of silicon carbide (SiC) using chemical vapor deposition [27]. The eventual interaction between local and global step bunching is not yet fully understood, and it is a matter of further investigations.

As we have already observed, the simulations show two main types of defects: local and extended ones. The first ones are associated to both vacancies and interstitials and are mainly connected to the *LSB*, whereas the second ones derive from nucleations on the terraces which are enhanced by the large terrace width. We remind again that this last condition can occur due to the substrate preparation, i.e. for small off-angle cuts, or

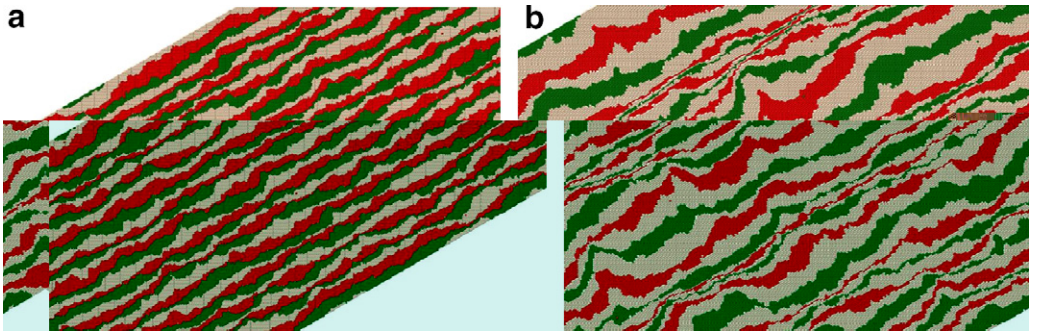


Fig. 9. Surface morphology comparison between 3C (left) and 4H (right) polytypes. Surface is shown from the $\langle 0\,0\,0\,1\rangle$ direction. *GSB* is present only on the 4H crystal. The system has a surface made up of $864 \times 864$ sites (refined lattice) distributed over 39 and 52 flat terraces, respectively, 18 units wide. Up to 200 layers have been grown, equivalent to $\sim 5 \times 10^8$ atoms, the deposition rate was set equal to $Gr = 5.2 \times 10^{-10}$ for both polytypes.

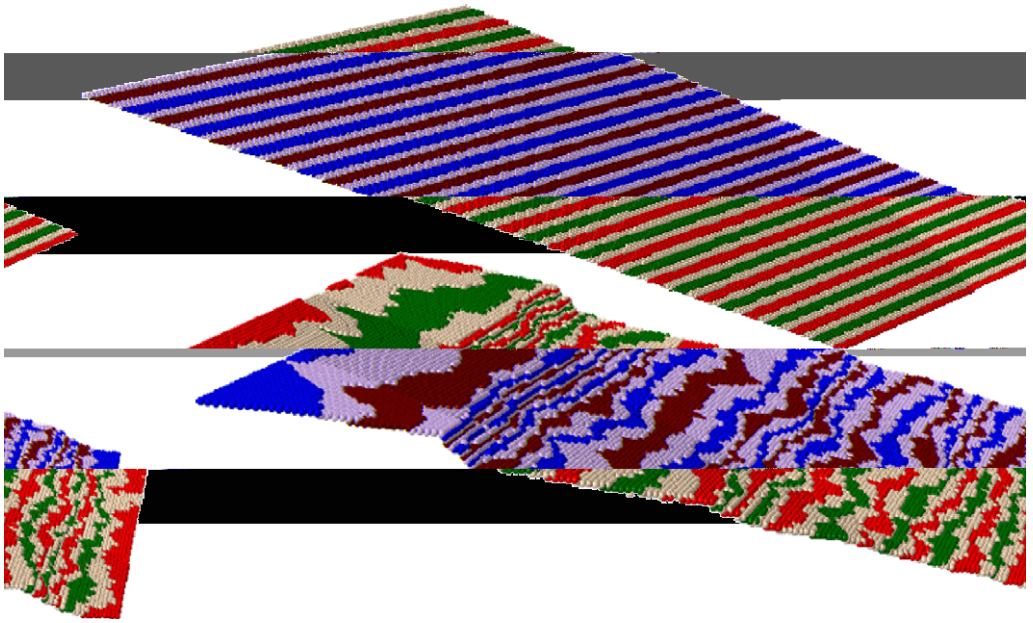

Fig. 10. Comparison between initial substrate and grown surface for the monocrystalline growth 150 layers for the 4H polytype, GSB and terrace width increase are clearly present. The system has a surface made up of $504 \times 252$ sites (refined lattice) distributed over 60 flat terraces 9 units wide. Up to 150 layers have been grown, equivalent to $\sim 6 \times 10^6$ deposed atoms, the deposition rate was set equal to $Gr = 2 \times 10^{-11}$.

dynamically during the growth process due to the *GSB*. We have, furthermore, observed that the generation of extended defects is "critical" in the sense that the growing film, during the deposition, passes abruptly from an almost perfect epitaxial structure to a highly defective structure (i.e. a polycrystalline one). While the generation of local defect is more uniform being constantly different from zero also during the early stages of the deposition process. These features can be observed comparing the two panels of Fig. 11 where the generation of local (left) and extended (right) defects as function of the number of the grown layers is shown. The derivative of the two functions is proportional to the defect density for each layer, which is almost constant only for local defects. This fact limits the possibility of growing thick epitaxial crystals for large terrace width (i.e. small off-angle cuts).

In Figs. 12 and 13, we show both the initial substrate and the final grown crystal using the same deposition conditions but the two different diffusion rules: KawR and BcR. As we could expect from the results obtained

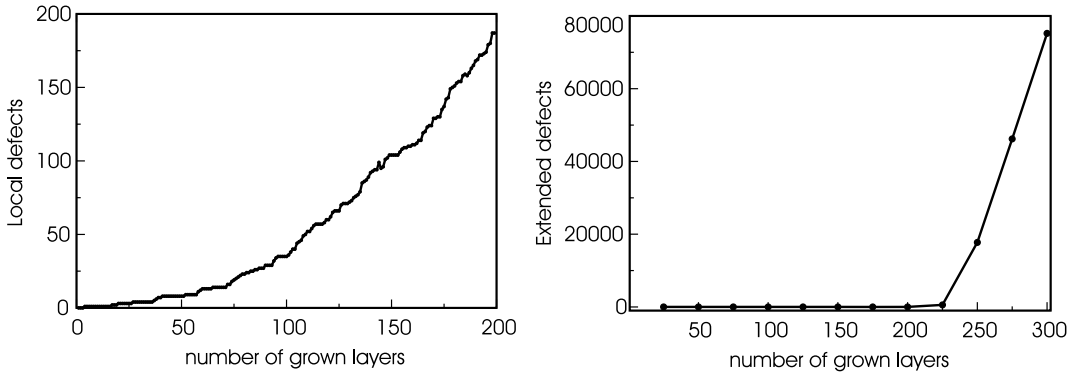


Fig. 11. Number of local defects (left panel) and extended ones (right panel) as function of the number of grown layers. The results derive from two different growth simulations: on the left panel the substrate had a surface made up of $270 \times 300$ sites (refined lattice) distributed over 30 flat terraces 6 units wide, the deposition rate was set equal to $Gr = 8 \times 10^{-10}$. On the right panel the substrate had a surface made up of $252 \times 150$ sites (refined lattice) distributed over 18 flat terraces 15 units wide (units of the refined inter-site distance), the deposition rate was set equal to $Gr = 8.5 \times 10^{-10}$.

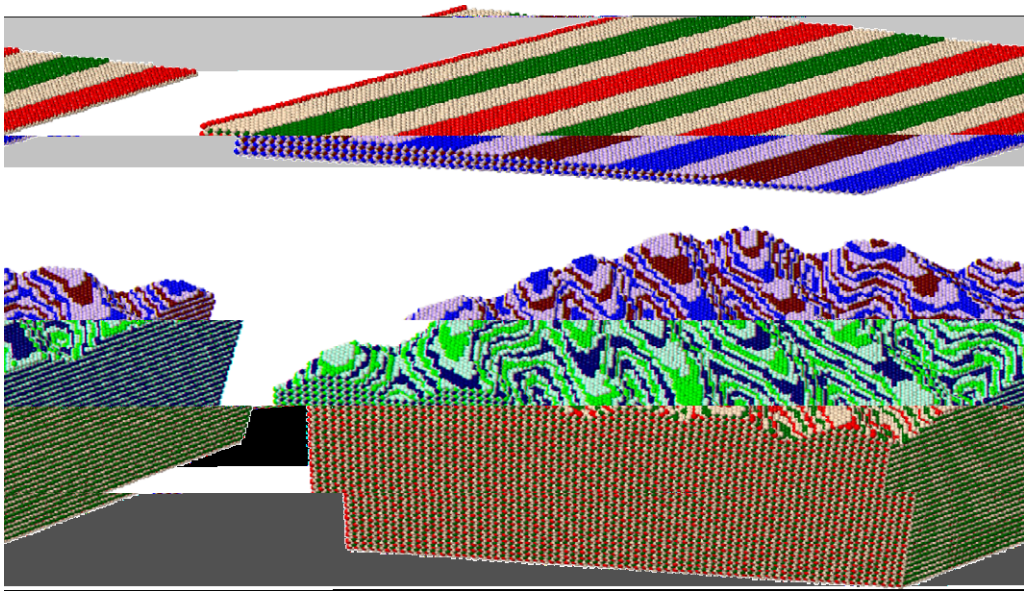

Fig. 12. 3D deposition simulation using the Kawasaki method. The system has a surface made up of $216 \times 216$ sites (refined lattice) distributed over 16 flat terraces 18 units wide (units of the refined inter-site distance). Up to 50 layers have been grown, equivalent to $\sim 7.7 \times 10^5$ deposed atoms, the deposition rate was set equal to $Gr = 3 \times 10^{-10}$. Step deformation is clearly present.

in the 2D case the simulation performed using the KawR show rougher steps. Beside this effect in the KawR simulation we observe also a morphological reconfiguration, with specific deformations along one of the six equivalent, minimum energy, $\langle 11\bar{2}0 \rangle$ directions. This morphological reconfiguration is more evident comparing the surface morphology of two grown crystals using the same physical conditions but off-angle cuts on the two equivalent directions $\langle 1\bar{1}00 \rangle$ (Fig. 13) and $\langle 11\bar{2}0 \rangle$ (Fig. 14). This phenomenon has been observed experimentally for the growth of SiC [15] and might explain why the $\langle 1\bar{1}00 \rangle$ off-angle cut direction has a higher grow rate limit in comparison with the $\langle 11\bar{2}0 \rangle$ one.

In order to analyze the growth in terms of defect quantity and defect type we consider separately two parameters: $D_L$ and $D_E$ which are proportional, respectively, to the density of local and extended defects. In Fig. 15, we show a comparison between the $D_E$ and $D_L$ dependence on the growth rate for the same grown

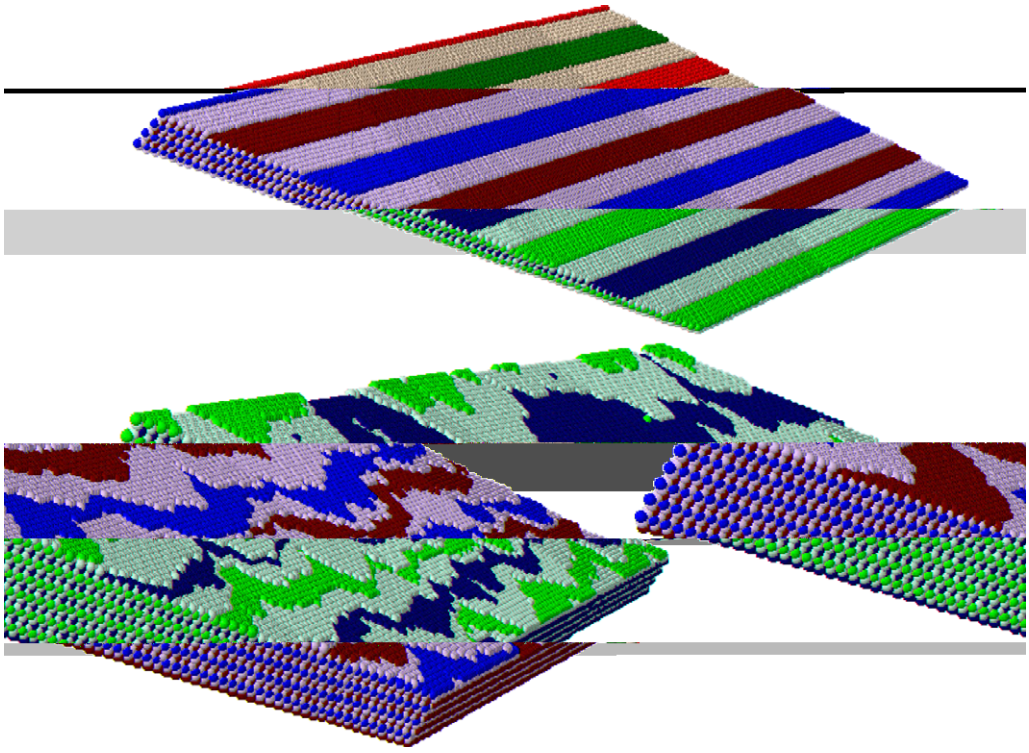

Fig. 13. 3D deposition simulation using the Bond Counting method with the off-cut angle direction $\langle 1\bar{1}00\rangle$. The system has a surface made up of $216 \times 216$ sites (refined lattice), distributed over 16 flat terraces 18 units wide (units of the refined inter-site distance). Up to 100 layers have been grown, equivalent to $\sim 1.5 \times 10^6$ deposed atoms, the deposition rate was set equal to $Gr = 3 \times 10^{-10}$, equal to the one used for the KawR (not all grown layers are shown for graphical convenience).

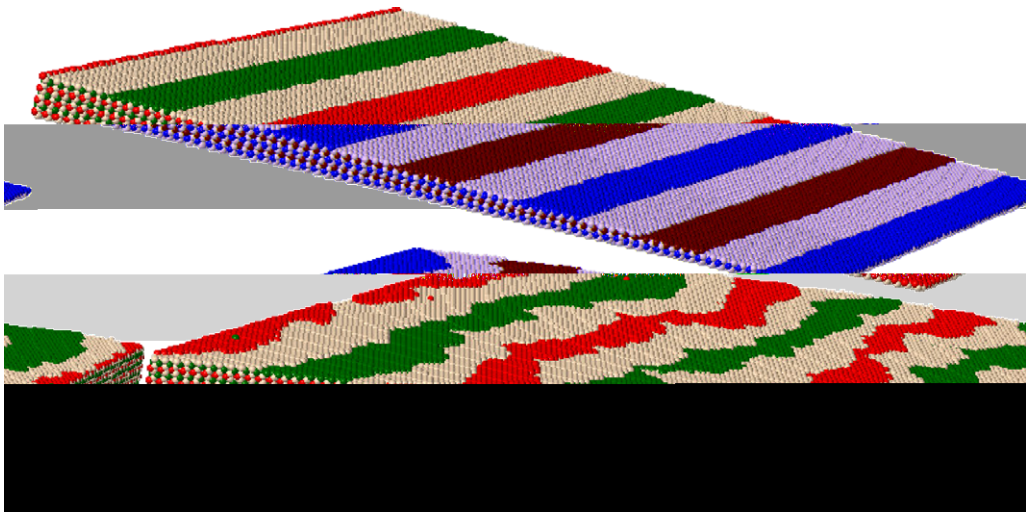

Fig. 14. 3D deposition simulation using the Bond Counting method with the off-angle cut direction $\langle 11\bar{2}0\rangle$. The system has a surface made up of $216 \times 216$ sites (refined lattice), distributed over 16 flat terraces 18 units wide (units of the refined inter-site distance). Up to 100 layers have been grown, equivalent to $\sim 1.3 \times 10^6$ deposed atoms, the deposition rate was set equal to $Gr = 3 \times 10^{-10}$, equal to the one used for the KawR (not all grown layers are shown for graphical convenience).

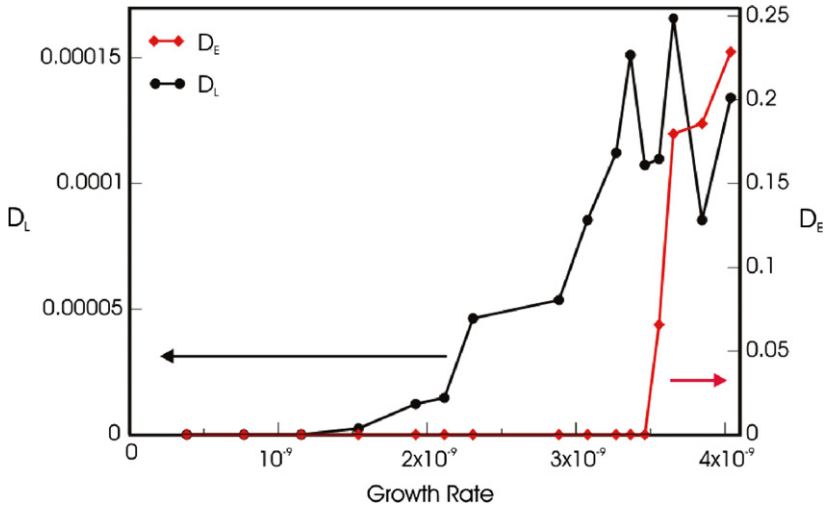


Fig. 15. Comparison between the $D_L$ and $D_E$ for the same grown crystal. The substrate had a surface made up of $270 \times 300$ sites (refined lattice) distributed over 30 flat terraces 6 units wide (units of the refined inter-site distance), up to 300 layers have been grown. An intermediate region between standard step-flow and 2D nucleation in clearly present.

crystal. From this figure we can identify three different deposition regimes: the standard epitaxial step-flow regime where both $D_E \sim 0$ and $D_L \sim 0$, the polycrystalline regime where $D_E > 0$ and $D_L > 0$, and an intermediate region where $D_E \sim 0$ and $D_L > 0$. This last region is of particular interest both from theoretical and practical point of view. In fact, in this region it is possible to grow thick epitaxial crystals with a controlled local defects density. We can denote this region as the "Defective Epitaxial Growth Regime". The extension of this region is related to the width of the terraces, eventually disappearing for large enough terraces (for our diffusion conditions this region disappears for terraces width greater than 18 units wide). In Fig. 16, we show the variation of both $D_E$ and $D_L$ both in terms of the growth rate and of the temperature for a large terrace case. As we could expect the density of both local and extended defects decrease when the temperature increases and the defective epitaxial regime cannot be evidenced. A schematic scenario obtained using a large number of the simulation results is reported in Figs. 17 and 18 where we show the "extended quality parameter" $Q_E$ obtained varying both the deposition rate the off-angle cut and the evolution rules. $Q_E$ is defined as

$$Q_E = \frac{\sum \mathrm{TotDep} - \sum \mathrm{WrongDep}}{\sum \mathrm{TotDep}} \tag{10}$$

where TotDep is the total number of deposed particles, and WrongDep is the number of particles with a different stacking sequence with respect to the substrate. By definition, $Q_E$ is equal to 1 for monocrystalline structures and $\sim 1/3$ for a completely random filling. As we can see there is a clear degradation of the grown crystal quality when increasing the deposition rate and decreasing the off-angle cut. This is a direct consequence of the higher nucleation probability (2D islands growth [18]) that we have in these conditions.

Finally, we can make some specific comparisons of the growth rate limit for different off-cuts with some analytical results based on the *BCF* theory of step flow. According to Ref. [18] we have the following close set of equations which relate the grow rate limit $Gr_{\lim}$ with the energetics of the grown material and the geometry of the substrate:

$$\lambda_S = a \exp\left(\frac{E_{des} - E_{Diff}}{2kT}\right) = a \exp\left(\frac{3\beta(R_q - 1)E_b}{2}\right) \tag{11}$$

$$\frac{n_{S0}}{\tau_S} = n_0 \theta_D \exp(-\beta E_{des}) = n_0 \theta_D \exp(-3\beta(R_q + 1)E_b) \tag{12}$$

$$Gr_{\lim} = \frac{(\alpha_{crit} - 1)h}{2n_0} \frac{n_{S0}}{\tau_S} \frac{4\lambda_S}{a\mathrm{Tw}} \tanh^{-1}\left(\frac{a\mathrm{Tw}}{4\lambda_S}\right) \tag{13}$$

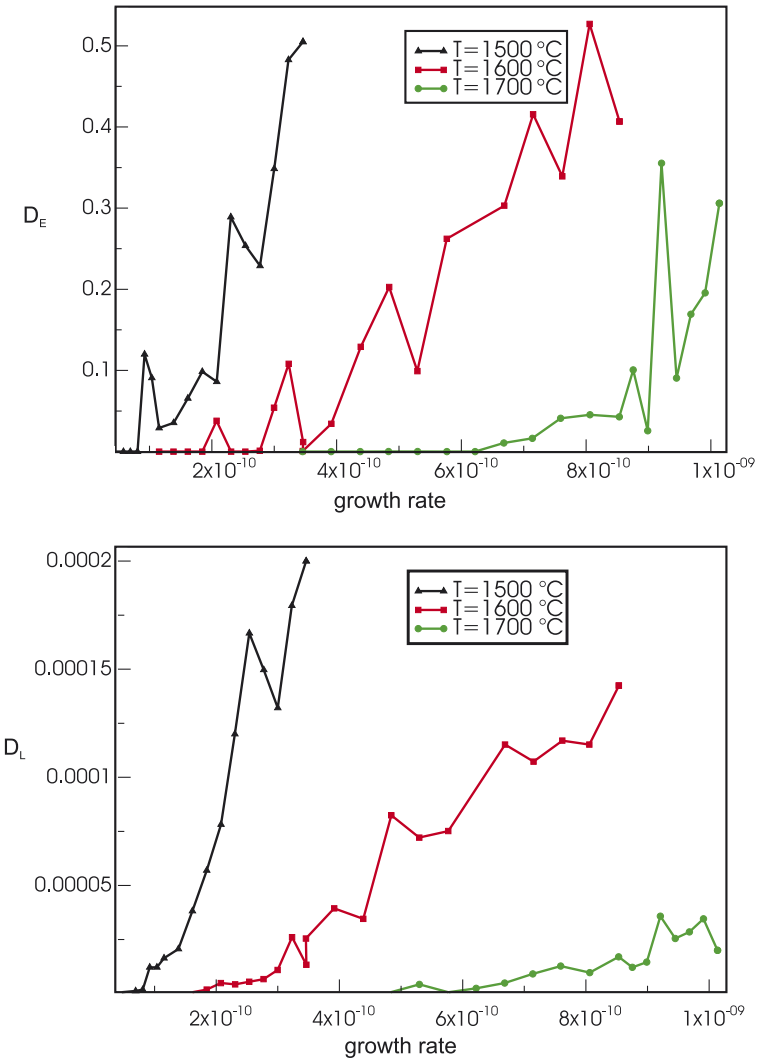


Fig. 16. Comparison between the $D_E$ (upper panel) and $D_L$ (lower panel) for different temperatures, fixing the terrace width (Tw = 24) and the bond strength ($E_b = 0.54$ eV). The substrate a surface made up of $330 \times 200$ sites (refined lattice) distributed over 15 flat terraces 24 units wide and up to 150 layers have been grown.

where Tw is the terrace width, $\lambda_s$ an average length for adatoms to migrate on a "step-free" surface before desorption, $h$ the step height, $a$ the inter-site distance in the (0001) plane (related to the original lattice, not the refined one), $n_0$ is the density of adatom site on the surface, $n_{S0}/\tau_S$ is the desorption flux, $R_q = E_{des}/E_{diff}$ the ratio between the desorption energy and the diffusion energy, $\theta_D$ is the Debye frequency and $\alpha_{crit}$ is the critical supersaturation ratio which, using Eq. (18) of Ref. [18], we find equal to $\alpha_{crit} = 3.9576$ for our energetic parameters. Following the specific material of Ref. [18] we set: $h = 0.252$ nm, $n_0 = 0.9 \times 10^7$ eV/μm$^2$, $a = 0.3086$ nm specific of the Silicon Carbide dimer. We furthermore set $R_q = 4$, $\beta E_b = 3.55$ and $\theta_D = 10^{13}$ s$^{-1}$ [19]. In Fig. 19, we compare this analytical result with the numerical growth rate limits using both the bond counting and the Kawasaki methods. The numerical estimate of the growth rate limit has been performed by means of the quality factor analysis, more specifically $Gr_{lim}$ is the growth rate value where $Q_E \geqslant 0.98$. As can be seen there is a good agreement between analytical and numerical estimates only for large terraces (low off-angle cuts), where both the roughness of the steps (which can eventually lead to LSB) and the step to step interaction can be neglected. These are some of the assumptions of the analytical model. Our *KLMC* method gives a significantly larger estimate of $Gr_{lim}$ in the small terrace limit but, as we

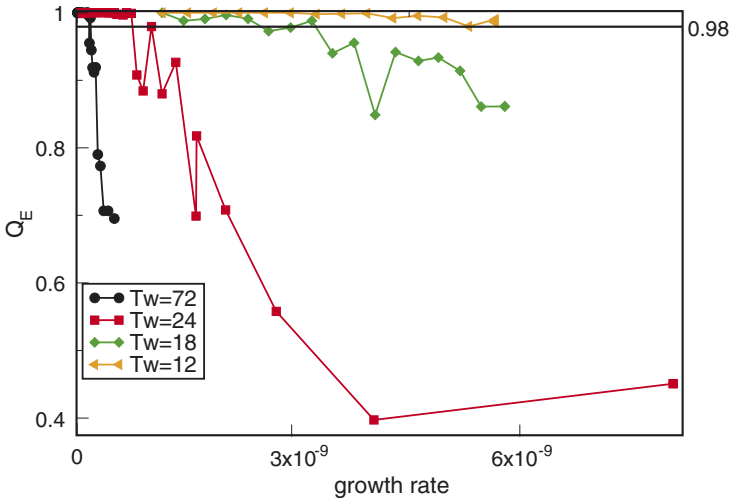


Fig. 17. Dependence of the "extended quality parameter" $Q_E$ on the growth rate and terrace width, using the bond counting rule. The value of $Q_E = 0.98$ has been used as threshold for the identification of the growth rate limit $Gr_{lim}$ of Fig. 19.

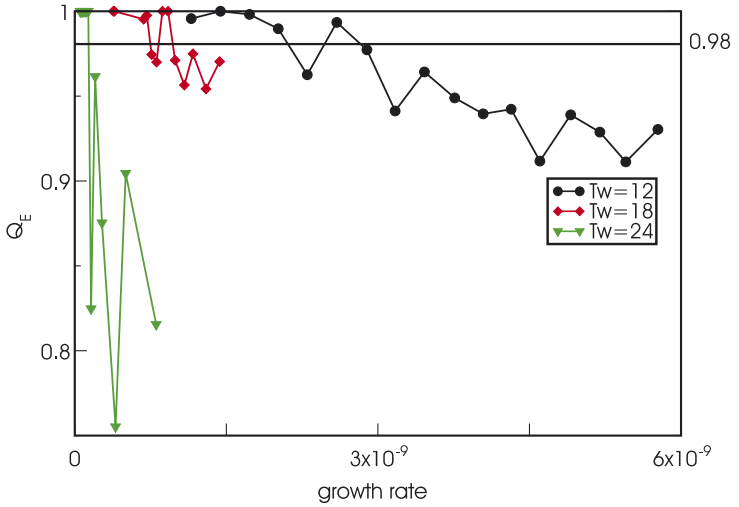


Fig. 18. Dependence of the "extended quality parameter" $Q_E$ on the growth rate and terrace width, using the Kawasaki rule. The value of $Q_E = 0.98$ has been used as threshold for the identification of the growth rate limit $Gr_{lim}$ of Fig. 19.

have already discussed, in this limit polytype mixing (i.e. island nucleation) is not the only degradation mechanism so that the $Q_E$ parameter could be insufficient to correctly define the overall quality of the grown crystal. In any case, a deeper understanding of the different mechanisms which affect the crystal quality *both* in the large and small terrace regimes are relevant for the applications to experimental homo-epitaxial crystal growth, since there is a large interest in studying the trade-off between nucleation growth rate, terrace width and crystal quality. We point out again that the $Gr_{lim}$ is the only average observable predicted by the analytic theory, whereas our method gives access also to further details (e.g. surface morphology, point defects, extended defective structures, etc.).

## 8. Discussion

This work meets a requirement; i.e. the predictivity extension of the kinetic simulations dedicated to epitaxial growth for the class of close packed crystalline structures. The motivation was the observation that, in spite

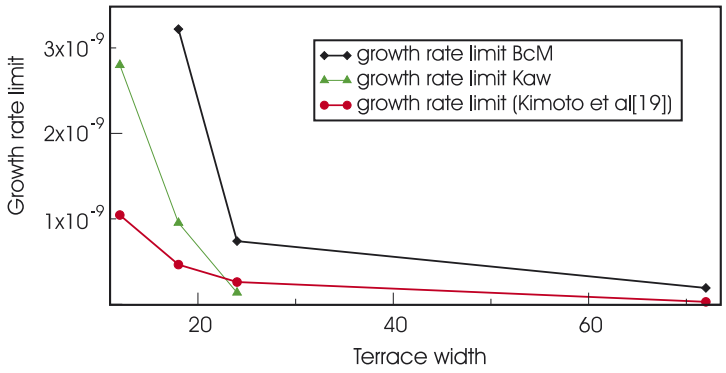


Fig. 19. Comparison between the growth rate limits for monocrystalline growth in terms of the terrace width obtained using the bond counting, the Kawasaki method and the analytical result of Ref. [18].

of an accurate mapping of the energetic, conventional kinetics approaches can address only single or limited aspects of the complex phenomenology, characterizing the growth process in dependence on the thermodynamic and geometric conditions. This is a structural limit and we can overcome it only releasing the restriction of using the conventional lattice of the material in study as the reference lattice of the stochastic method. However, adopting a refined lattice or super-lattice in the KLMC method poses serious questions on the refinement limit, the implementation efficiency, the recovering of unpredictable and unphysical features during the simulations.

We have demonstrated that, for the case of close packed structures, we can formulate an efficient and reliable KLMC, including in our refined lattice all the three categories of highly symmetric sites (usually called A, B, C) which characterize the one-dimensional stacking of close packed lattices. Our code aims at investigating the morphology of the defective configurations eventually forming during the growth processes. This work mainly poses the attention on the methodology itself. However, the features and the potentiality of the method seem really appealing for future applications to real substances and processes.

A first consideration arises when simply dealing with the energetic mapping: the inclusion of all the highly symmetric sites of the stacked structure is necessary for a reliable mapping, since *ab initio* calculations have revealed [25,26] that only considering all these sites it is possible to take into account the potential barriers for the adatom diffusion on a free surface. Therefore, extending this consideration, our methodology opens new perspectives when addressing a complete multi-scale study of the growth process using joined *ab initio*, MD and KLMC approaches. Indeed, in general, only using a KLMC based on super-lattices the detailed atomistic mechanisms of the system evolution (e.g. surface diffusion, step diffusion, attachment/detachment events, crossing of Schwoebel barriers, etc.) evidenced by *ab initio* and MD calculations can be properly recovered in KLMC simulations.

Further considerations are related to the kinetic features, which are accessible to our simulations and offer an ideal ground for the comparisons with the experimental analysis of the surface and bulk morphology in real samples during and after a growth process. The impact of the island nucleation, which preferentially occurs in systems with large terraces in the high deposition regime, is correctly evaluated since islands of the two symmetries complementary to the terrace could nucleate and evolve. The interaction between the step and the two kinds of islands is completely different. Islands with the same symmetry of the step do not alter substantially the step effective kinetics since they are easily incorporated by the step. The encounter between the step and islands with different symmetry strongly modifies the effective step kinetics, since the interaction between the two structures tend to change the symmetry of the adatom bounded to the island. Indeed, the encounter event could cause a strong deformation of the step (in the case of relatively small islands) or the stabilization of a region with complementary symmetry (in the case of large islands) on the exposed terrace and the consequent growth of a polycrystalline structure.

Besides the islands nucleation we demonstrate that our approach allows also to consider the other mechanisms, namely the Global Step Bunching and the Local Step Bunching, which can lead to a progressive deterioration of the epitaxial quality of the growing substrate as consequence of a fault in the stacking order. The

point like (LSB) and the extended (GSB) encounter between two or more adjacent steps show the proper morphological character and can be investigated in dependence of the substrate geometry and the deposition conditions. Their relevance is proper of the wide angle (small terrace) substrate geometry. However, maybe the more relevant feature of our code is the concurrent access to all the degradation mechanism of the stacking order so that the correlation between, island nucleation, LBS and GSB can be rightly investigated (e.g. GBS event could lead to the enlargement of some terraces boosting island nucleation, or nucleation events of small islands can deform the step boosting LSB and so on). Finally, we can also characterize the generation of point like defects, denoting the Defective Epitaxial Growth Regime, which is a fundamental parameter for the quality of the experimentally grown epitaxial films.

Future work will be devoted to the calibration of the code, considering particular materials and deposition processes, and to the verification of its predictivity in term of correlation between the deposition conditions and the defects character; e.g. using for the comparison experimental Atomic Force Microscopy analysis of the film surface.

## Acknowledgements

This work is partially supported from the Public–Private Laboratory Project DM23176 (art.12 08/08/2000) financed from the Ministry of University and Research of Italy.

## References

[1] A.R. Verma, P. Krishna, Polymorphysm and Polytypism in Crystals, John Wiley & Sons, New York, 1966.
[2] H.S. Kong, J.T. Glass, R.F. Davis, J. Appl. Phys. 64 (1988) 2672.
[3] N. Kurada, K. Shibabara, W.S. Yoo, S. Nishino, H. Matsunami, in: S. Furukawa (Ed.), Extended Abstracts of the 19th Conference on Solid State Devises and Materials, Tokyo, Business Center for Academic Societies, Tokyo, Japan, 1987, p. 227.
[4] W.K. Burton, N. Cabrera, F.C. Frank, Philos. Trans. Roy. Soc. London Ser. A 43 (1951).
[5] M. Avrami, J. Chem. Phys. 8 (1940) 212–240.
[6] Phillip J. Stout, J. Vac. Sci. Technol. A 16 (1998) 3314.
[7] F. Gao, E.J. Bylaska, W.J. Weber, L.R. Corrales, Phys. Rev. B 64 (2001) 245208.
[8] P. Torelli, F. Sirotti, P. Ballone, Phys. Rev. B 68 (2003) 205413.
[9] S. Tan, P. Lam, Phys. Rev. B 60 (1999) 8314.
[10] M. Strobel, A. La Magna, S. Coffa, Nucl. Instr. Meth. Phys. Res. B 186 (2002) 339.
[11] Hanoch Mehl, Ofer Biham, Itay Furman, Majid Karimi, Phys. Rev. B 60 (1999) 2106.
[12] A. La Magna, S. Coffa, Comp. Mat. Sci. 17 (2000) 21.
[13] <http://www.math.sci.hiroshima-u.ac.jp/m-mat/MT/emt.html>.
[14] M.E.J. Newman, G.T. Barkema, Monte Carlo Methods in Statistical Physics, Clarendon Press, Oxford, 1999, p.305.
[15] A. Nakajima, H. Yokoya, Y. Furukawa, H. Yonezu, J. Appl. Phys. 97 (2005) 104919.
[16] R.L. Schwoebel, E.J. Shipsey, J. Appl. Phys. 37 (1966) 3682.
[17] Noboru Ohtani, Masakazu Katsuno, Jun Takahashi, Hirokatsu Yashiro, Masatoshi Kanaya, Phys. Rev. B 59 (1999) 4592.
[18] T. Kimoto, H. Matsunami, J. Appl. Phys. 75 (1994) 850.
[19] Actually, using these energetic parameters, the diffusion length $\lambda_S$ and the desorption flux $n_{S0}/\tau_S$ assume the same range of values of those estimated for the SiC crystal growth of [18].
[20] T. Kimoto, A. Itoh, H. Matsunami, Appl. Phys. Lett. 66 (1995) 3645.
[21] N. Ohtani, M. Katsuno, J. Takahashi, H. Yashiro, M. Kanaya, Phys. Rev. B 59 (1999) 4592.
[22] M. Syväjärvi, R. Yakimova, E. Janzén, J. Phys. Condens. Mat. 11 (1999) 10019.
[25] A. Catellani, Phys. Rev. B 71 (2005) 075303.
[26] O. Trushin, A. Karim, A. Kara, T.S. Rahman, Phys. Rev. B 72 (2005) 115401.
[27] A. Fissel, J. Crystal Growth 212 (2000) 438.